

Real-time studies of thin film growth: Measurement and analysis of X-ray growth oscillations beyond the anti-Bragg point

S. Kowarik^{1,2,a}, A. Gerlach^{1,2}, M.W.A Skoda^{1,2}, S. Sellner¹, and F. Schreiber^{1,2}

¹ Universität Tübingen, Institut für Angewandte Physik, 72076 Tübingen, Germany

² Oxford University, Physical and Theoretical Chemistry, Oxford OX1 3QZ, UK

Abstract. Monitoring X-ray growth oscillations, i.e. temporal oscillations of the X-ray reflectivity during thin film growth, is an important technique for *in-situ* and real-time characterization of heteroepitaxy. Here we demonstrate the simultaneous acquisition and analysis of not only one, but a set of growth oscillations in a wide range of the reciprocal space (q -space). Importantly, the combined information of these growth oscillations removes ambiguities inherent in the analysis of a single (anti-Bragg) oscillation. Wide q -range measurements also enlarge the accessible parameter range in film thickness and roughness, as measurements at optimized q -values exhibit a larger amplitude and lower damping during growth. As an example we analyze oscillations at $q = 1/2, 2/3, 3/4 \dots, q_{\text{Bragg}}$ during molecular beam deposition of the organic semiconductor diindenoperylene using kinematic scattering theory. From this we derive the growth mode and the surface roughening with film thickness.

1 Introduction

Understanding and controlling the growth of thin films is of great importance for many areas of science and technology, while at the same time understanding growth phenomena is also of interest as an important branch of statistical physics [1–3]. Generally, growth is a dynamic non-equilibrium phenomenon so that *real-time* and *in-situ* measurement techniques during growth are ideal, because they allow one to follow the growth *dynamics* as opposed to post-growth measurements at only one final thickness, potentially only after a post-growth re-organization process.

Scattering techniques are particularly suited for real-time observation, as they are non-invasive. Various scattering techniques including RHEED [4–6], helium scattering [7–9], and X-ray scattering [10–21] have been used for *in-situ* and *real-time* growth studies. RHEED is most commonly used to study growth under UHV conditions but in some cases can be damaging, e.g. for growth of organics. Moreover, the data analysis for electron scattering is not always as straight-forward as for X-ray scattering. Optical techniques such as for example ellipsometry [22, 23] or differential reflectance spectroscopy [24] have also been employed for real-time monitoring of film growth.

In this work we focus on X-ray scattering, which offers flexibility in the sample environment (e.g. vacuum, air, liquids), yields high q -space resolution, and can be analyzed in most cases by simple single scattering (kinematic) theory. Different approaches in X-ray scattering have been used to monitor film growth. One possibility is to simply monitor the growth of Bragg

^a *Present address:* University of California, Department of Chemistry, Berkeley, CA 94720, USA.

reflections [25,26], which, while useful for identifying structural changes (in-plane and out-of-plane) and to some degree growth kinetics, does not give direct information about the filling of individual crystalline layers in the film. For following layer-by-layer growth, it is therefore common practice to follow “growth oscillations” which originate from the consecutive filling of crystalline layers with atoms or molecules [14]. From these oscillations the details of layer nucleation, layer filling, and film roughening can be derived. To set the present work in perspective, we note that growth oscillations at the so-called anti-Bragg point ($q_{anti} = 1/2 \cdot q_{Bragg}$) [13,14,27–30], but also at other points in q -space [19,20,31] have been used to obtain quantitative information about the sequential filling of crystalline layers, as well as the Ehrlich-Schwoebel barrier for interlayer transport [12]. In general though it is not obvious which point in q -space is best suited to observe growth oscillations with strong modulations. Further difficulties arise also in the theoretical analysis of the anti-Bragg oscillations when determining in which layer atoms are incorporated because of ambiguities in between all odd/all even atomic monolayers. For example anti-Bragg oscillations may persist despite an unbounded increase of the surface width [32], which could be misinterpreted as a layer by layer growth when only observing the anti-Bragg point.

In this work we demonstrate that it is possible to *simultaneously* acquire correlated growth oscillations at several points in q -space including the anti-Bragg point, which allows one to resolve ambiguities in the analysis and makes it possible to follow the growth also during roughening of the film. We establish that there is a pronounced change in growth mode of the organic semiconductor diindenoperylene from layer-by-layer growth to 3d-island growth. This paper is organized as follows: In section 2 we give a description of anti-Bragg oscillations including substrate interference effects. In section 3 we discuss the simulation of oscillations at other q -points and subsequently use the theoretical analysis to fit a set of experimental growth oscillations in section 4.

2 X-ray growth oscillations at the anti-Bragg point

2.1 Origin of X-ray reflectivity oscillations during growth

X-ray growth oscillations are time dependent, periodic modulations of the *specular* X-ray reflectivity during growth. The temporal oscillations are due to alternating constructive and destructive interference between X-ray reflections from the (growing) top surface, the crystal lattice, and the buried interface between film and substrate (Figure 1a).

We want to stress that there exist also other mechanisms for growth oscillations, which we briefly describe for differentiation only. Interference effects governing X-ray oscillations are *not* identical to the interference effects dominating RHEED and Helium scattering. X-rays penetrate the sample and therefore oscillations also have contributions of buried lattice planes and interfaces, whereas electrons and Helium have large scattering cross-sections making them very sensitive to only the near-surface region/morphology. This leads to qualitatively different phenomena: for example anti-Bragg X-ray oscillations in heteroepitaxy show a period of *two* monolayers while RHEED and Helium scattering exhibit an oscillation period of *one* monolayer, as these two techniques are sensitive to the surface roughness, which oscillates between smooth (for a filled layer) and rough (for a half filled layer) [34]. Also, for X-rays there exists diffuse scattering due to this surface roughness oscillation but this effect is generally much smaller than oscillations due to interference effects. For a full understanding of X-ray growth oscillations the diffuse scattering can be measured together with the specular oscillations (see for example refs. [30,35]). In our work we have established that the diffuse oscillations are much weaker than oscillations due to interference (<5%) and therefore are neglected.

For the calculation of X-ray reflectivity we use the single scattering (kinematic) approximation which assumes that multiple scattering of X-rays can be neglected; this assumption is not valid close to the critical angle α_c where dynamical (Parratt) theory is needed [36] but the single scattering approximation describes the region $\alpha \gg \alpha_c$ well where growth oscillations are commonly observed.

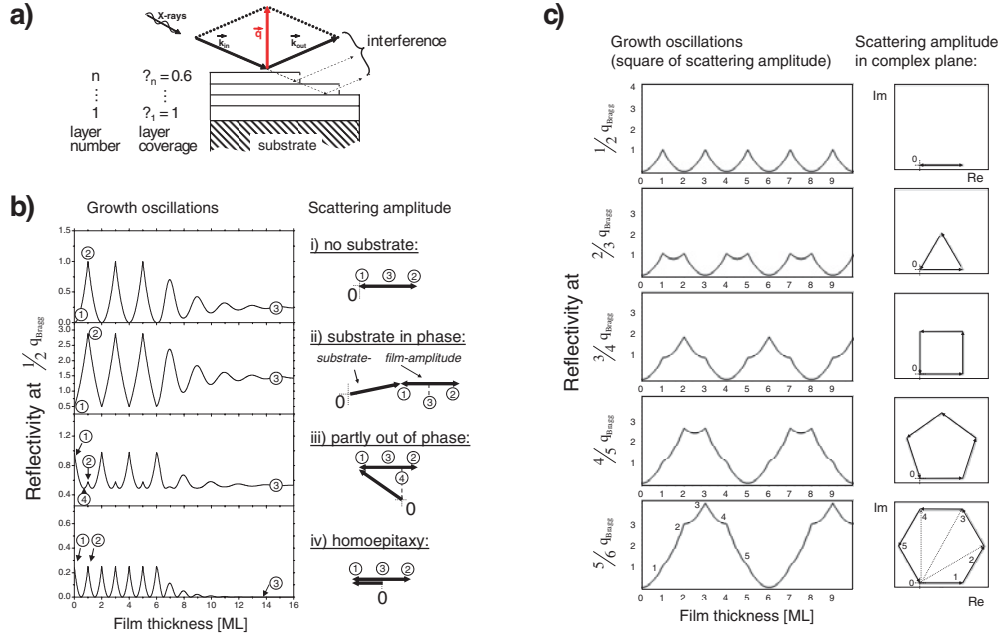


Fig. 1. a) Scattering geometry for specular reflectivity measurements of a crystalline ad-layer on a substrate. b) Simulation of anti-Bragg ($= 1/2 q_{Bragg}$) oscillations including substrate scattering. Adding a substrate scattering amplitude to the film scattering amplitude drastically changes $1/2$ -Bragg (anti-Bragg) growth oscillations: i) no substrate scattering; ii) changed shape and height of the oscillations (note different scale); iii) inversion (maxima instead of minima), and new side maxima; iii) a period of one monolayer. c) Left panel: Growth oscillations exhibit different shape and oscillation period for different points in q -space (without substrate). As a convenient illustration of the origin of the oscillation shape, the right panel shows the scattering amplitudes and their relative phase for each q -value. The scattering amplitude of one monolayer corresponds to a vector in the complex plane, while the total scattering amplitude is given by a vector from the origin 0 to the point corresponding to the current stage in growth as exemplified for the first five monolayers at $q = 5/6 q_{Bragg}$.

Interference effects can then be calculated in kinematic approximation by summing over the scattering amplitudes of every crystalline layer and the substrate, taking into account the relative phase (see Figure 1a). The reflected intensity of the growing thin film is then given by:

$$I_{reflected}(t) = \left| A_{substrate}(q) \cdot e^{i\Phi(q)} + f(q) \cdot \sum_n \theta_n(t) \cdot e^{i \cdot n \cdot q \cdot d} \right|^2. \quad (1)$$

$A_{substrate}(q)$: substrate scattering amplitude

$f(q)$: atomic/molecular form factor of an ad-layer

$\Phi(q)$: phase between substrate and ad-layer scattering

n : layer number;

θ_n : fractional coverage of the n^{th} -layer (0-zero coverage, 1-filled layer);

q : X-ray wavevector transfer upon reflection;

d : lattice spacing within the crystalline thin film.

Inserting the anti-Bragg condition ($q_{anti} = 1/2 \cdot q_{Bragg}$) into Equation (1) the contributions of odd and even layers have an alternating sign and therefore growth oscillations occur (see Figure 1b), as consecutive layers interfere destructively – even monolayers (second, fourth, ... layer) exactly cancel the scattering contribution of odd monolayers (first, third, ... layer). In real growth scenarios the oscillations do not continue indefinitely, but are damped with time (that is film thickness) because the layer-by-layer growth typically gives way to a roughening of

the surface. Importantly, the growth oscillations are strongly affected by the substrate on which the film is growing and one usually cannot neglect the substrate scattering. The oscillation period, the shape, and amplitude of oscillations are affected by the substrate scattering as discussed in the following.

2.2 Analysis of complex oscillation patterns due to substrate interference

The interference between substrate and film scattering substantially changes the form of the growth oscillations as shown in Figure 1b). Different representative cases for possible phase relationships between substrate and adlayer scattering are shown in Figure 1b) and the resulting anti-Bragg growth oscillations have been calculated according to Equation (1). Compared to growth oscillations without a substrate contribution in Figure 1b) the oscillation amplitude between points ① and ② can increase significantly if the substrate scatters in phase (Figure 1b, panel ii), an effect similar to homodyne amplification in electronics/optics which for a suitable choice of substrate can be used to increase the detection sensitivity and time resolution. Also the shape of the oscillations is altered and even new side-maxima can appear at point ② as shown in panel iii) in Figure 1b). We note that the saturation level ③ after the oscillations have been damped out strongly depends on the interference between substrate and film reflectivity as shown in Figure 1b), and can also be used to extract information about the scattering amplitudes and phase.

For a quantitative analysis of X-ray scattering intensities in the presence of a substrate the unknown parameters $A_{substrate}(q)$, $f(q)$, and $\Phi(q)$ in Equation (1) have to be determined so that the filling factors $\theta_n(t)$ can be derived. Using three experimental quantities – intensities at the first maximum I_{max} at point ①, minimum I_{min} at point ②, and saturation level of the growth oscillation ($I(t \rightarrow \infty) = I_{saturation}$) at point ③ – the three unknown parameters entering the scattering theory can be uniquely determined and subsequently the $\theta_n(t)$ can be fitted to extract information about growth.

Homoepitaxy as special case of heteroepitaxy

For the case of homoepitaxy, that is for the film and substrate lattice constants d and form factors $f(q)$ being identical, the ‘side’ maxima ② are as strong as the ‘main’ maxima ①. This can be derived from equation (1) by inserting the geometric sum of a semi-infinite lattice for the substrate reflectivity:

$$I_{reflected}(t) = \left| -f(q) \cdot \frac{1}{e^{-i \cdot q \cdot d} - 1} + f(q) \cdot \sum_n \theta_n(t) \cdot e^{i \cdot n \cdot q \cdot d} \right|^2$$

$$\text{for } \underline{q=\pi/d} \left| f(q) \cdot \left(-\frac{1}{2} + \sum_n \theta_n(t) \cdot e^{i \cdot n \cdot \pi} \right) \right|^2. \quad (2)$$

As main and side maxima cannot be distinguished, anti-Bragg oscillations in homoepitaxy exhibit a period of *one* monolayer (see Figure 1b) panel iv), in contrast to heteroepitaxy, where one oscillation occurs for every *two* monolayers (see refs. [14, 37, 38]).

3 Growth oscillations beyond the anti-Bragg condition

Growth oscillations can not only occur at the anti-Bragg point but also at every point in q -space other than the Bragg condition [20]. In general, the anti-Bragg condition is *not* the point with the largest oscillation amplitude or the longest duration of oscillations, so that other points may be preferable for measurements depending on the type of information sought.

3.1 $1/2$ -, and $2/3$ -, $3/4$ -, $4/5$ -, $5/6$ -Bragg growth oscillations

Figure 1c) shows the time evolution of the specular X-ray reflectivity calculated according to Equation (1) at q -values of $1/2 \cdot q_{Bragg}$, $2/3 \cdot q_{Bragg}$, $3/4 \cdot q_{Bragg}$, $4/5 \cdot q_{Bragg}$. The reflected intensity $I_{reflected}$ is shown in the left panel of Figure 1c), while the scattering amplitudes and phase for each layer is represented as an arrow in the complex plane in the right panel. For the clarity of presentation ideal layer-by-layer growth is assumed and also scattering from the substrate is neglected, but of course substrate scattering can be included in the description treating it similarly to section 2.2.

For the $2/3$ -Bragg ($q = 2/3 \cdot q_{Bragg}$) condition again the scattering from consecutively growing layers leads to an oscillating signal, repeating itself every three layers, as the scattering amplitudes describe a triangle in the complex plane (see Figure 1c). For the $3/4$ -, $4/5$ - ... Bragg conditions the oscillation amplitude gets longer, until for the Bragg condition all layers add up in phase and there are no growth oscillations but a quadratic increase in scattering intensity.

In Figure 1c), the scattering amplitude has been set to be of unit length independent of q . In general though, the scattering amplitude changes with q , with the details obviously depending on the material grown and the exact shape of its form factor $f(q)$. Therefore the oscillation strength usually is smaller for large q , because the scattering amplitude and the form factor $f(q)$ decrease strongly for larger q -values.

3.2 Relation to growth modelling

Once the free parameters within the scattering theory ($A_{substrate}(q)$, $f(q)$, and $\Phi(q)$) have been determined the X-ray reflectivity oscillations can be calculated for any given set of $\theta_n(t)$, which in general are parameterised using a physical model of growth processes. A full discussion of these models is obviously beyond the scope of this paper [1,2]. Rather, in order to illustrate the main points and the relation to the experiments, we limit ourselves to an intentionally simple and very transparent model that can be solved analytically to yield the occupation of the individual lattice-planes $\theta_n(t)$ on a *fixed lattice*, i.e. neglecting strain. In the diffusive growth model after Cohen et al. [5] the rate for a jump from layer $n + 1$ to n is proportional to an effective rate constant k_n , the uncovered fraction of layer $n + 1$, and the available space in layer n (Equation (3)). In the present work the k_n have been varied for each layer, so that a transition from layer-by-layer growth to mound-growth and the associated damping of growth oscillations can be modelled.

$$\frac{d\theta_n}{d(t/\tau)} = (\theta_{n-1} - \theta_n) + k_n(\theta_{n+1} - \theta_{n+2})(\theta_{n-1} - \theta_n) - k_n(\theta_{n-2} - \theta_{n-1})(\theta_n - \theta_{n+1}). \quad (3)$$

- θ_n : fractional coverage of the n^{th} -layer;
- τ : completion time for one monolayer;
- k_n : effective rate for interlayer transport.

4 Experimental case study

We use the example of thin film growth of the organic semiconductor diindenoperylene (DIP [39]), $C_{32}H_{16}$, an organic semiconductor to illustrate the data acquisition and analysis of real-time growth oscillations. The organic thin films have been grown by molecular beam deposition in a portable UHV-chamber [40] at a base pressure of $\sim 1 \cdot 10^{-9}$ mbar. The UHV chamber can be mounted onto an X-ray diffractometer and is equipped with an effusion cell, a thickness monitor, and a Be-window transparent for X-rays, so that *in-situ* and *real-time* experiments are possible. In our experiments DIP was evaporated onto silicon wafers with native oxide at $\sim 130^\circ\text{C}$ substrate temperature with a rate of $1 \text{ \AA}/\text{min}$. The X-ray reflectivity data was measured at the European Synchrotron Radiation facility (ESRF) at beamline ID10B with an

X-ray wavelength of 0.963 \AA . The typical time resolution for angular dispersive X-ray scattering is between ~ 1 s for the measurement of growth oscillations at one point in q space, and < 120 s for real-time mapping of a wide q -range mainly limited by the motor movement times.

This experimental time resolution of 1–120 s is well suited to study slow growth processes (ranging from 10–1000 s for deposition of a monolayer) as well as de-wetting phenomena, and techniques such as energy dispersive reflectometry show potential for higher time resolution [11,41,42]. With acquisition times of ~ 2 min per reflectivity scan, it is possible to collect the reflectivity $I(q, t)$ as a function of time t as well as of q during DIP growth. Figure 2a) gives an overview over such a data set $I(q, t)$ during deposition of a crystalline thin film of DIP. The X-ray reflectivity can be seen to evolve from the bare silicon oxide reflectivity (back of the graph, that is $time = 0$) to the reflectivity of a 285 \AA film of DIP with the most prominent feature being the growing Bragg reflection of DIP (at $q_{Bragg} = 0.377 \text{ \AA}^{-1}$, in the front of graph).

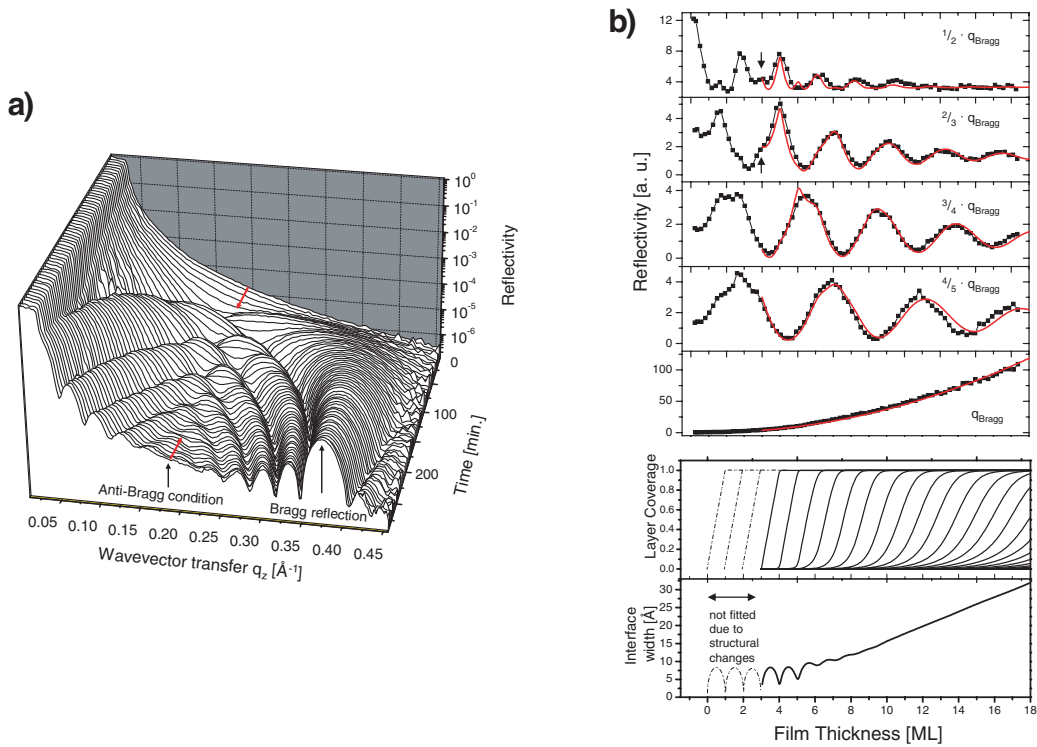


Fig. 2. a) Real-time evolution of the reflectivity during growth of the molecule diindenoperylene (DIP) on silicon oxide. With increasing deposition of DIP on silica a Bragg-reflection for the DIP-film appears. An intricate pattern of finite thickness oscillations develops with time, which causes the reflected intensity at a fixed q value to oscillate with time. b) Growth oscillations at different q -values during evaporation of DIP (subset of data shown in a). A simultaneous fit to all growth oscillations (red), allows one to extract the evolution of the interface width (film roughness) and layer coverages during deposition.

Reflectivity curves at certain times $I(q, t = \text{fixed})$ can be analysed using the Parratt formalism [43,44], but to study the time evolution of growth here we focus on cuts through this 3d data set along the time direction $I(q = \text{fixed}, t)$. Figure 2b) shows the resulting growth oscillations from cuts through Figure 2a) at the following q -values: $1/2$ (anti-Bragg), $2/3$, $3/4$, $4/5$ as well as the Bragg condition $q_{Bragg} = 0.378 \text{ \AA}^{-1}$. As expected from the simulations of growth oscillations in section II the oscillation is fastest at the anti-Bragg point and gets slower for q -values closer to the Bragg condition.

The damping of the oscillations is strongest at the anti-Bragg point, as shown in Figure 2b). Therefore an obvious advantage of acquiring oscillations at other q -points is the ability to follow the growth and roughening of the film for longer. The first three monolayers were not included in the fits, as the form factor $f(q)$ and the lattice spacing change as previously established in ref. [45]. Simultaneous fitting of all growth oscillations with the same $\theta_n(t)$ and k_n leads to the theoretical reflectivity curves shown in Figure 2b). The $\theta_n(t)$ contain the complete information out-of-plane structure during film formation and it is possible to use the $\theta_n(t)$ to calculate e.g. the interface width (surface roughness) as shown in Figure 2b) (bottom).

Importantly the interface width increases significantly from the 6th layer onwards, showing the marked transition from layer-by-layer growth to strong roughening in DIP growth.

5 Conclusions

In conclusion we have shown that monitoring growth oscillations is a useful technique to determine the growth mode. Anti-Bragg oscillations allow to follow fast growth processes with monolayer resolution and allow for a simple interpretation. As shown, interference effects between substrate reflections and reflections of the thin film complicate the shape of oscillations but also allow for homodyne amplification of the oscillations and additional information about the phase of the reflections can be obtained. We further note that growth oscillations are not restricted to the anti-Bragg condition and it is possible to optimize the signal by choosing the appropriate q -value for growth oscillations. At the anti-Bragg point the oscillation amplitude is usually not maximised and the dampening with increasing film roughness is strongest, so that other q -values may be favourable for experiments. Further, simultaneous acquisition of data at several points in q -space removes the ambiguity between odd layers $\theta_{2n+1}(t)$ and all even layers $\theta_{2n}(t)$ which is inherent to analysis of only anti-Bragg oscillations.

Experimentally we have demonstrated for DIP growth that it is possible to acquire and analyze wide q -range reflectivity data *in-situ and in real-time* during thin film growth. From this data we determine the evolution of the partial layer coverages $\theta_n(t)$, and the roughness during growth and find that there is a marked transition from layer-by-layer growth to island growth.

We gratefully acknowledge experimental support by L. Cavalcanti, and O. Konovalov, as well as discussions with J. Krug and U. Pietsch. We would like to thank the EPSRC and DFG for financial support.

References

1. A. Pimpinelli, J. Villain, *Physics of Crystal Growth* (Cambridge University Press, Cambridge, 1998)
2. J. Krug, Adv. Phys. **46**, 139 (1997)
3. A.C. Dürr, F. Schreiber, K.A. Ritley, V. Kruppa, J. Krug, H. Dosch, B. Struth, Phys. Rev. Lett. **90**, 016104 (2003)
4. W. Braun, L. Däweritz, K.H. Ploog, Phys. Rev. Lett. **80**, 4935 (1998)
5. P.I. Cohen, G.S. Petrich, P.R. Pukite, G.J. Whaley, A.S. Arrott, Surf. Sci. **216**, 222 (1989)
6. P. Turban, L. Hennen, S. Andrieu, Surf. Sci. **446**, 241 (2000)
7. R. Kunkel, B. Poelsema, L.K. Verheij, G. Comsa, Phys. Rev. Lett. **65**, 733 (1990)
8. L. Casalis, M.F. Danisman, B. Nickel, G. Bracco, T. Toccoli, S. Iannotta, G. Scoles, Phys. Rev. Lett. **90**, 206101 (2003)
9. S. Söhnchen, S. Lukas, G. Witte, J. Chem. Phys. **121**, 525 (2004)
10. H. You, R.P. Chiarello, H.K. Kim, K.G. Vandervoort, Phys. Rev. Lett. **70**, 2900 (1993)
11. B.K. Kellerman, E. Chason, D.P. Adams, T.M. Mayer, J.M. White, Surf. Sci. **375**, 331 (1997)
12. A.C. Mayer, R. Ruiz, H. Zhou, R.L. Headrick, A. Kazimirov, G.G. Malliaras, Phys. Rev. B **73**, 205307 (2006)
13. A.C. Mayer, R. Ruiz, R.L. Headrick, A. Kazimirov, G.G. Malliaras, Org. Electron. **5**, 257 (2004)

14. E. Vlieg, A.W. Denier van der Gon, J.F. van der Veen, J.E. Macdonald, C. Norris, *Phys. Rev. Lett.* **61**, 2241 (1988)
15. B. Krause, F. Schreiber, H. Dosch, A. Pimpinelli, O.H. Seeck, *Europhys. Lett.* **65**, 372 (2004)
16. H.H. Teng, P. Fenter, L. Cheng, N.C. Sturchio, *Geochim. Cosmochim. Acta* **65**, 3459 (2001)
17. P.C. Dai, Z. Wu, T. Angot, S.K. Wang, H. Taub, S.N. Ehrlich, *Phys. Rev. B* **59**, 15464 (1999)
18. C.L. Nicklin, C. Norris, P. Steadman, J.S.G. Taylor, P.B. Howes, *Phys. B: Cond. Matter* **221**, 86 (1996)
19. W. Braun, B. Jenichen, V.W. Kaganer, A.G. Shtukenberg, L. Däweritz, K.H. Ploog, *Surf. Sci.* **525**, 126 (2003)
20. E. Weschke, C. Schüßler-Langeheine, R. Meier, G. Kaindl, C. Sutter, D. Abernathy, G. Grübel, *Phys. Rev. Lett.* **79**, 3954 (1997)
21. M.V.R. Murty, A.J. Couture, B.H. Cooper, A.R. Woll, J.D. Brock, R.L. Headrick, *J. Appl. Phys.* **88**, 597 (2000)
22. M. Kytka, A. Gerlach, F. Schreiber, J. Kovac, *Appl. Phys. Lett.* **90**, 131911 (2007)
23. V. Burtman, Y. Ofir, S. Yitzchaik, *Langmuir* **17**, 2137 (2001)
24. H. Proehl, T. Dienel, R. Nitsche, T. Fritz, *Phys. Rev. Lett.* **93**, 097403 (2004)
25. F. Schreiber, A. Eberhardt, T.Y.B. Leung, P. Schwartz, S.M. Wetterer, D.J. Lavrich, L. Berman, P. Fenter, P. Eisenberger, G. Scoles, *Phys. Rev. B* **57**, 12476 (1998)
26. R.L. Headrick, S. Kycia, Y.K. Park, A.R. Woll, J.D. Brock, *Phys. Rev. B* **54**, 14686 (1996)
27. R.G.V. Silfhout, J.W.M. Frenken, J.F.V.D. Veen, S. Ferrer, A. Johnson, H. Derbyshire, C. Norris, J.E. Macdonald, *J. Phys.: Condens. Matter* **1**, 213 (1989)
28. C. Boragno, F. BuatierdeMongeot, G. Costantini, U. Valbusa, R. Felici, D.M. Smilgies, S. Ferrer, *Phys. Rev. B* **65**, 153406/153401 (2002)
29. M. Beckers, N. Schell, R.M.S. Martins, A. Mucklich, W. Moller, L. Hultman, *J. Appl. Phys.* **99**, 034902 (2006)
30. J. Alvarez, E. Lundgren, X. Torrelles, S. Ferrer, *Surf. Sci.* **464**, 165 (2000)
31. K.A. Edwards, P.B. Howes, J.E. Macdonald, T. Hibma, T. Bootsma, M.A. James, *Surf. Sci.* **424**, 169 (1999)
32. J. Krug, T. Michely, *Islands, Mounds and Atoms: Patterns and Processes in Crystal Growth Far From Equilibrium* (Springer, Heidelberg, 2004)
33. H. Kiessig, *Ann. Phys.* **402**, 769 (1931)
34. J.A. Stroschio, D.T. Pierce, R.A. Dragoset, *Phys. Rev. Lett.* **70**, 3615 (1993)
35. A. Fleet, D. Dale, A.R. Woll, Y. Suzuki, J.D. Brock, *Phys. Rev. Lett.* **96**, 055508 (2006)
36. L.G. Parratt, *Phys. Rev.* **95**, 359 (1954)
37. I.K. Robinson, P.J. Eng, P.A. Bennett, B. DeVries, *Appl. Surf. Sci.* **60-61**, 498 (1992)
38. C. Norris, *Phil. Trans. R. Soc. Lond. A* **344**, 557 (1993)
39. DIP was purchased from Institut für PAH-Forschung, Greifenberg, Germany
40. K.A. Ritley, B. Krause, F. Schreiber, H. Dosch, *Rev. Sci. Instrum.* **72**, 1453 (2001)
41. E. Chason, T.M. Mayer, A. Payne, D. Wu, *Appl. Phys. Lett.* **60**, 2353 (1992)
42. S. Kowarik, A. Gerlach, W. Leitenberger, J. Hu, G. Witte, C. Wöll, U. Pietsch, F. Schreiber, *Thin Solid Films* **515**, 5606 (2007)
43. J. Als-Nielsen, D. McMorrow, *Elements of Modern X-Ray Physics* (Wiley, New York, 2001)
44. M. Tolan, *X-ray Scattering from Soft-matter Thin Films: Materials Science and Basic Research* (Springer, Berlin, London, 1999)
45. S. Kowarik, A. Gerlach, S. Sellner, F. Schreiber, L. Cavalcanti, O. Konovalov, *Phys. Rev. Lett.* **96**, 125504 (2006)